xxx (xxxx) xxx

Contents lists available at ScienceDirect

Biomaterials Advances

journal homepage: www.journals.elsevier.com/materials-science-and-engineering-c

In-vitro viability of bone scaffolds fabricated using the adaptive foam reticulation technique

James Winnett [a,*], Neeraj Jumbu [b], Sophie Cox [b], Greg Gibbons [a], Liam M. Grover [b], Jay Warnett [a], Mark A. Williams [a], Claire E.J. Dancer [a], Kajal K. Mallick [a]

[a] Warwick Manufacturing Group, University of Warwick, Coventry CV4 7AL, United Kingdom
[b] School of Chemical Engineering, University of Birmingham, Edgbaston, Birmingham B15 2TT, United Kingdom

ARTICLE INFO

Keywords:
Foam Reticulation
Scaffolds
Bone regeneration
Hierarchical porosity
In-vitro assay
Mechanical strength

ABSTRACT

The adaptive foam reticulation technique combines the foam reticulation and freeze casting methodologies of fabricating bone reparative scaffolds to offer a potential alternative to autografts. For the first time this paper studies the effect of processing on the mechanical properties and *in-vitro* cell growth of controllably generating a hierarchical structure of macro- (94 ± 6 to 514 ± 36 μm) and microporosity (2–30 μm) by the inclusion of camphene as a porogen during processing. Scaffolds were produced with porogen additions of 0–25 wt%. Porosity values of the structures of 85–96% were determined using the Archimedes technique and verified using X-ray Computed Tomography. The strength of the hydroxyapatite scaffolds, 5.70 ± 1.0 to 159 ± 61 kPa, correlated to theoretically determined values, 3.71 ± 0.8 to 134 ± 12 kPa, calculated by the novel incorporation of a shape factor into a standard equation. Fibroblast (3T3) and pre-osteoblast (MC3T3) cell growth was found to be significantly ($P < 0.005$) improved using 25 wt% porogen. This was supported by increased levels of alkaline phosphatase and was thought to result from greater dissolution as quantified by increased calcium levels in incubating media. The combination of these properties renders adaptive foam reticulation-fabricated scaffolds suitable for non-structural bone regenerative applications in non-load bearing bone defects.

1. Introduction

Bone reparative scaffolds offer an alternative to traditional autografting techniques [1]. These have been developed to overcome the limitations such as lack of available tissue, donor site morbidity and the risk of potentially fatal musculoskeletal infections [1]. Although there are many methods designed to fabricate synthetic scaffold structures, none fulfil all of the requirements proposed to enable optimised tissue ingrowth whilst maintaining mechanical stability. In particular, scaffolds should have an open 3D interconnected porous network of macropores (100–900 μm) that enables cells, nutrients and metabolites to fully infiltrate the structure [2,3]. Additionally, a network of micropores (2–20 μm) can enhance vascularisation of the construct [4], whilst surface roughness provides cells with attachment sites [5] and may increase the surface area available for surface dissolution. The aim with regenerative medical scaffolds is to generate a suitable hierarchical structure replicating that of bone, although this has not been achieved despite many years of research.

Macroporosity can be achieved using a range of techniques that can produce macropores within the prescribed limits (100–900 μm), which include solvent casting/particulate leaching [6], freeze casting [7,8], foam reticulation [9], gelcasting [10], sol-gel technology [11], and additive manufacturing (AM), including Binder Jetting [12,13], Powder Bed Fusion [14,15], Material Jetting [16] and robocasting [17,18]. Representative features of typically used scaffold manufacturing techniques are briefly summarised in Table 1.

These techniques enable the porosity of scaffolds to be regulated, with the pore size dependant on the technique although all within the range of human cancellous bone (70–90%) [20]. Although there is less control over the distribution of pores, the conventional manufacturing techniques typically offer greater osteogenic potential, demonstrated through *in-vitro* and *in-vivo* studies assessing the numbers of osteoblast-like cells, including MC3T3 [25] and MG63 [9], and expression of alkaline phosphatase (ALP) [9,25,28,29]. Conversely AM scaffolds offer greater control over the macroporous structure [26], but elicit less of a biological response, such as bone marrow stromal cell (bMSC) number

* Corresponding author.
E-mail address: j.winnett.1@warwick.ac.uk (J. Winnett).

https://doi.org/10.1016/j.bioadv.2022.212766
Received 6 September 2021; Received in revised form 22 February 2022; Accepted 14 March 2022
Available online 25 March 2022

[30].

However, none of these offer the potential to controllably and simultaneously produce microporosity, which has a positive effect on the viability of scaffolds [18,19], alongside the macroporous network. Particularly, developing a structure whereby a hierarchical porous network spanning multiple orders of magnitude can be controllably manufactured presents a significant challenge.

By combining foam reticulation and freeze casting techniques, the Adaptive Foam Reticulation (AFR) method facilitates the realisation of controllable macro- and microporosity [37,38]. Macroporosity is generated through the replication of a suitable template whilst microporosity is achieved by freeze drying a suitable sacrificial porogen. Previously, this has been used to generate a controlled hierarchical structure from hydroxyapatite (HA) [38], Bioglass [39], and titanium and titanium-aluminium-vanadium alloy [40]. Whilst the crystallography and porous structure of the scaffolds has been evaluated previously [37–40], in this study the porosity, compressive strength, and cell growth evaluation of the structures is studied in detail to produce a fuller assessment of the suitability of AFR fabricated structures for use as bone regenerative scaffolds.

2. Materials & methodology

2.1. Adaptive foam reticulation

Scaffolds were fabricated for this investigation from HA using the AFR technique as detailed elsewhere [38]. Briefly, the precursor biomaterial was mixed into a slurry combining Dolapix CE64 (Sigma, UK) as a dispersant, methylcellulose (Sigma, UK) as a binder, and distilled water. To generate microporosity, camphene (Sigma, UK) was dissolved in dimethylcarbonate (Sigma, UK) to produce a porogen and added to the slurry at 0, 5, 10, 20 and 25 wt% ratios.

The slurry was impregnated onto polyurethane templates (Recticel, UK) with two porosities (45 and 90 pores per inch (ppi)) up to 5 times, with the slurry allowed to dry at room temperature (20 °C) for 30 min between coats, before being dried in air at room temperature for 24 h. To evaluate the effect of the freeze-drying temperature on the micropore formation, templates were coated once and dried in a Labconco FreeZone 2.5 Liter Freeze Dry System (Labconco, USA), equipped with a Small Clear Drying Chamber. Samples were held at the desired temperature for 4 h, with the scaffold temperature measured using k-type thermocouples (Omega Engineering Ltd., UK). Sublimation of the ice crystals was achieved using a controlled heating regime under pressure (0.133 mbar).

Once dried, all scaffolds were subjected to a controlled firing schedule with a heating ramp rate of 0.5 °C/min to 500 °C where it was held for 3 h to burn out the polymer, before a subsequent ramp at the same rate to 1350 °C where it was held for 3 h to sinter the final construct before cooling at 1 °C/min to room temperature.

2.2. Porous structure

To investigate the 3D nature of the structure, selected samples underwent X-ray micro-computed tomography (XCT) analysis using an Xradia 520 Versa (Zeiss, Germany), equipped with an X-ray sealed source (40 kV, 3 W), a CCD detector, quartz filter, and lens optic magnification. For low resolution scans (5 μm) to measure the macroporosity only, 0.4× optical magnification was used, with 3201 projections and an exposure time of 15 s. High resolution scans (0.8 μm) to determine the microporosity levels were recorded using 4× optical magnification with 4500 projections and an exposure time of 38 s. Analysis was undertaken using Avizo 8.1 (Visualizations Sciences Group, FEI, USA), using the Iso-50% value. It was assumed for the low-resolution scans that the structures contained no micropores, hence all struts were assumed to be solid during post-processing. The surface area was determined using the in-built features of the software.

2.3. Porosity

Bulk density and porosity (P_o) of the scaffolds (n = 3) was determined using the Archimedes method on a Mettler Toledo MS204 balance equipped with MS-DNY-4 density kit (Mettler Toledo, UK), with calculations for the scaffold density [41] obtained using Eq. (1):

$$P_o = 1 - \frac{\rho_{scaffold}}{\rho_{solid}} \quad (1)$$

where ρ_{solid} is the bulk density of the material, 3156 kg/m^3 [42] and $\rho_{scaffold}$ is calculated using Eq. (2):

$$\rho_{scaffold} = \rho_{water} \cdot \frac{W_d}{W_w - W_{su}} \quad (2)$$

where ρ_{water} is the absolute density of water, 998 kg/m^3 [43], and W_d, W_w and W_{su} are the dry, wet and submerged masses of the scaffold respectively.

Table 1
Comparison of pore size, porosity, compressive strength and biological response from different bone scaffold manufacturing techniques.

Method	Pore size (μm)	Porosity (%)	Compressive strength (MPa)	Biological response	Ref
Cancellous bone	1–3500	10–90	2–23	n/a	[20,21]
Dry methods	n/a	n/a	0.11–0.23	n/a	[22,23]
Phase separation/freeze casting	8–200	30–75	2–36	Enhanced MC3T3 and ALP	[7,24,25]
Replication techniques	Foam dependent (10−1000)	<95	0.3–8.4	Enhanced MG63, ALP and other gene groups	[9,26]
Gelcasting	0.1–1000	<90	2–32.6	Enhanced ALP and osteoblast like cells	[10,27,28]
Sol-gel techniques	Graded (0.037–1000)	50–70	2–20	Increased osteogenic cell markers	[11,29]
Solvent casting/particulate leaching	Particle dependent (5–600)	50–90	0.3–9.3	Enhanced osteoblast growth	[6]
Binder Jetting	Feature >10 Layer >20	Tailored (30–80)	0.2–45	bMSC decreased, ALP enhanced	[13,30]
Powder Bed Fusion	Feature >10 Layer >76	Tailored (30–80)	2–31	No change	[15,31]
Vat Polymerisation	Feature: 1–100 Layer >1	Tailored (30–80)	1.3–56	Similar at best	[13,32]
Robocasting	Feature >30 Layer >30	Tailored (30–80)	2–20	n/a	[33,34]
Material Jetting	Feature >200 Layer >0.4	Tailored (30–80)	n/a	n/a	[35,36]

2.4. Compressive strength

Compression tests were performed on cylindrical HA samples of 15 mm height with 10 mm diameter. These were loaded into a custom, in-house built stainless steel holder attached to an Instron 5800R tensile tester (Instron, UK) equipped with a 1 kN load cell. Testing was undertaken with a cross head speed of 2 mm/min on scaffolds produced from both templates, with 5 coats, after sintering to 1350 °C and with 2 different porogen contents (0 and 25 wt%). The results were correlated with theoretical values obtained using Eq. (3), which has previously been used to calculate the strength of porous scaffolds [44]. To accommodate the effect of the microporosity, a shape factor (μ_o) normally used with microporous bulk structures has been incorporated, as shown in Eq. (4) [45].

$$\frac{\sigma_{theor}}{\sigma} = 0.2 \cdot \mu_o \cdot \left(\frac{\rho_{scaffold}}{\rho_{solid}}\right)^3 \frac{1 + \left(t_p/t_s\right)^{\frac{3}{2}}}{\sqrt{1 - \left(t_p/t_s\right)^{\frac{3}{2}}}} \quad (3)$$

where σ_{theor} is the theoretical compressive strength, σ is the yield stress of the bulk material, $\rho_{scaffold}/\rho_{solid}$ is the relative density, t_p/t_s is the ratio of pore to strut size and:

$$\mu_o = \frac{\frac{\pi}{4}\left(1 - \frac{t_m}{t_p}\right)^3}{1 - \frac{\pi}{4}\left(1 - \frac{t_m}{t_p}\right)^3} \quad (4)$$

where t_m/t_p is the ratio of micropore to macropore size.

2.5. In-vitro evaluation

The viability of similar scaffolds has already been shown to be greater than that of a commercially available porous HA disc (CellSupports, UK) [38], so in this study further analyses were undertaken to determine the effect of incorporating a porogen. In particular, the aim was to determine whether producing microporosity had a positive effect on cell viability. Thus scaffolds fabricated as previously documented [38] were used as the controls.

Analysis of the cell compatibility of the ceramics was undertaken on scaffolds produced with 5 coats of the slurry and sintered to 1350 °C. Assays were performed using 3T3 cells (NIH, Sigma, UK) cultured in monolayer to the 23rd passage on scaffolds produced with 0, 5, 10, 20 and 25 wt% porogen, whilst those with 0 and 25% porogen were also subjected to analyses with MC3T3 cells (ECACC, Sigma, UK) cultured in monolayer to the 18th passage. Prior to analysis, all scaffolds were disinfected by submersion in 70 vol% ethanol for 1 h, before air drying for 1 h. All cell evaluation was undertaken by seeding scaffolds with 2.5×10^5 cells, which were cultured in Dulbecco's Modified Eagle's Medium (DMEM) (Sigma, UK) supplemented with 10 vol% bovine serum (Sigma, UK), 2 vol% $_L$-glutamine (Sigma, UK), 1 vol% Penicillin/Streptomycin (Pen/Strep) (Sigma, UK) and 2.4 vol% 4-(2-hydroxyethyl)-1-piperazine-1-ethanesulfonic acid (HEPES) buffering solution (Fluka, UK).

Viability of 3T3 cells was analysed using a live/dead assay using Calcein AM (Invitrogen, UK) and Propidium Iodide (PI) (Invitrogen, UK). Viability was assessed after 1 and 3 days by replacing the media with 3 ml phosphate buffered solution (PBS) containing 10 μg/ml calcein AM and 10 μg/ml PI. Images were obtained at 1 and 3 days using an Axiolab microscope connected to an Axiocam ICM-1 camera with Zen software (Zeiss, Germany), with excitation/emission at 488 nm/525 nm for calcein AM and 525 nm/620 nm for PI.

The number of viable 3T3 and MC3T3 cells was quantified by 3-(4,5-dimethylthiazol-2-yl)-2,5-diphenyl tetrazolium bromide (MTT) after 1, 4 and 7 days. MTT reagent was added at 10 vol% of the culture media and incubated at 37 °C for 4 h. The formazan crystals were dissolved in 0.1 N acidic isopropanol for 45 mins with gentle agitation every 15 mins. Spectrophotometric measurements were taken at 570 nm using a GloMax -Multi Detection System spectrofluorometer (Promega, UK).

The impact of the hierarchical porous structure obtained using AFR on the level of osteogenic differentiation on scaffolds seeded with 3T3 and MC3T3 cells was measured using an ALP assay after 1, 4 and 7 days following the manufacturer's protocol provided with a SensoLyte pNPP Alkaline Phosphatase Assay Kit *Colorimetric* (Cambridge Bioscience, UK). The absorbance was detected at 410 nm on the GloMax -Multi Detection System.

The level of calcium dissolution was assessed by measuring the calcium in the culture solution after 1, 4 and 7 days following the manufacturer's protocol provided with a Cayman Chemical Calcium Assay kit (Cambridge Bioscience, UK). Disinfected scaffolds were incubated in PBS and DMEM separately at 37 °C, with measurements taken at 570 nm on the GloMax Multi Detection System. Incubation was undertaken in both solutions to allow the elimination of any effects on cell growth due to the incubating solution.

2.6. Statistical analyses

All statistical analysis was carried out using Student's *t*-test and Tukey's Pairwise Correlation. The differences were considered as significant at levels of $P < 0.05$.

3. Results

3.1. Structure

All structures exhibited a high degree of porosity of 85–96% when measured by the Archimedes method (Fig. 1). Generally, the level of porogen inclusion had a small effect on overall porosity (<1%), however incorporating 25% porogen significantly ($P < 0.005$) increased the overall porosity by up to 3%, although this was not consistently observed. Meanwhile, increasing the number of coats from 1 to 5 led to a significant ($P < 0.005$) average decrease in porosity of 2.1%, up to a maximum of 11%. Scaffolds from the 45 ppi template were approximately 5% more porous than those from the 90 ppi template. These trends were supported by XCT analysis of selected scaffolds, as shown in Table 2.

The effects of varying the porogen content has been investigated using XCT on selected scaffolds, as shown in Fig. 2. Furthermore, there was good correlation (<8%) between measurements of the porosity obtained by the XCT data and the Archimedes method, as shown in Table 2. The microporosity within the struts was also measured from

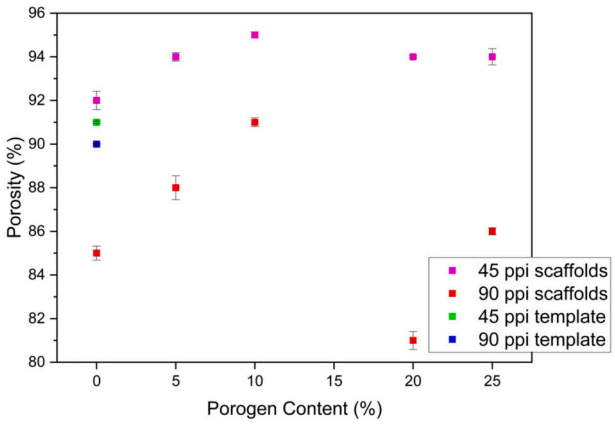

Fig. 1. Mean (± σ_e) porosity values for structures (n = 3) fabricated from both 45 and 90 ppi templates and with varying (0, 5, 10, 20 and 25%) camphene loading in the slurry with 5 coats of the slurry and sintered to 1350 °C. The values for the foam templates used to fabricate the scaffolds are also presented.

Table 2
Mean (± σ_e) porosity values obtained using Archimedes Principle (n = 3), and total and strut porosities (%) and surface area measurements obtained using XCT for scaffolds produced using both templates, with 5 coats of the slurry, sintered to 1350 °C and with 0%, 5%, 10%, 20% and 25% camphene loading in the slurry.

Template	Porogen content	Porosity (%) (Archimedes)	Total porosity (%) (XCT)	Strut porosity (%) (XCT)	Surface area (mm^2/mm^3)
45 ppi	Template	91 ± 0.05	n/a	n/a	n/a
	0%	92 ± 0.42	89.8	36.8	55.1
	5%	94 ± 0.20	87.0	39.6	36.1
	10%	95 ± 0.15	91.5	43.6	67.3
	20%	94 ± 0.06	87.5	29.5	38.4
	25%	94 ± 0.37	87.6	51.1	37.9
90 ppi	Template	90 ± 0.04	n/a	n/a	n/a
	0%	85 ± 0.32	91.6	28.5	122.6
	5%	88 ± 0.55	94.0	23.0	200.0
	10%	91 ± 0.20	92.5	34.4	139.7
	20%	91 ± 0.41	93.2	38.1	134.1
	25%	86 ± 0.16	89.5	37.2	56.6

high resolution XCT, with values of 23–51%, due to the removal of the template as can be seen by the hollow regions of struts, also shown in Fig. 2.

3.2. Compressive yield stress

The yield stress of samples obtained through testing to failure indicated that the ultimate compressive strength was dependant on the amount of porogen in the sample and the template from which it was used (Table 3). Samples from the 90 ppi template had higher yield stresses, of 144 ± 22 and 159 ± 61 kPa when fabricated with 0 and 25% porogen, respectively, compared to values of 18.4 ± 1.9 and 5.70 ± 1.0 kPa when fabricated from the 45 ppi template. Furthermore, the values for the scaffolds from the 90 ppi template without porogen, and both sets of samples from the 45 ppi template matched the theoretical values of 134 ± 12, 16.5 ± 4.5 and 3.71 ± 0.8 kPa calculated from Eqs. (3) and (4). However, the experimental value was significantly ($P < 0.0005$) greater for the samples produced from the 90 ppi template with 25% porogen than the theoretical value of 16.5 ± 1.7 kPa.

Due to the correlation between theoretical and experimental values, the compressive strength of all remaining samples was estimated using Eqs. (3) and (4) rather than destructively testing them. The yield stress of all samples was increased with a higher number of coats of the slurry on the template, and when using the 90 ppi template compared to the 45 ppi template (Table 3). Porogen content and freezing temperature also had a limited effect, although freezing to the lowest temperature led to weaker structures, as shown in Supplementary S1, with the theoretical compressive strength of scaffolds 2–140 kPa.

3.3. Cell viability

Analysis using Calcein AM/PI indicated a high level (>95%) of cell viability after 1 and 3 days when seeded on scaffolds produced from both templates, regardless of whether or not porogen was incorporated in the slurry. The cells have become elongated in morphology, indicating that they were attaching to the struts, as shown in the confocal microscopy images in Fig. 3.

To determine the effect of microporosity on scaffold viability, the 3T3 and MC3T3 cell number was quantified after 1, 4 and 7 days using the MTT assay, Fig. 4. When seeded with 3T3 cells, the number reduced significantly after 1 day, although the reduction was minimised by incorporation of the porogen. The only level of porogen content that consistently increased the cell number compared to the scaffold produced without porogen was 25 wt% ($P < 0.005$), although some positive effects were also seen with a 5 wt% inclusion. Furthermore, although the cell number was similar regardless of the template, incorporating a porogen had a greater effect ($P < 0.01$) on cell growth numbers for scaffolds generated from the 45 ppi foam than for the 90 ppi foam.

When seeding MC3T3 cells, there was a slight increase in the cell number after 1 day compared to the number seeded, indicating a

Table 3
Comparison of mean ± σ_e theoretical yield stresses and mean ± σ_e (n = 5) values obtained through testing of selected samples to failure.

Sample	Porosity (%)	Yield stress (kPa)	Theoretical strength (kPa)
0% porogen, 90 ppi	85 ± 0.32	144 ± 22	134 ± 12
0% porogen, 45 ppi	92 ± 0.42	18.4 ± 1.9	16.5 ± 4.5
25% porogen, 90 ppi	86 ± 0.16	159 ± 61	16.5 ± 1.7
25% porogen, 45 ppi	94 ± 0.37	5.70 ± 1.0	3.71 ± 0.8

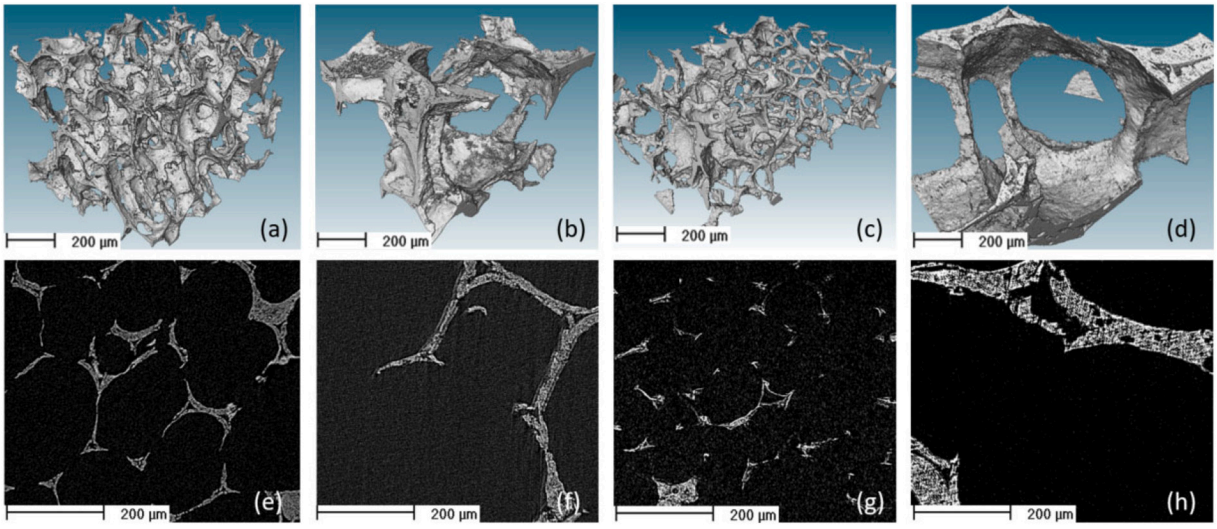

Fig. 2. XCT images of scaffolds produced *via* AFR, with 3D renderings of the macrostructure, (a), (b), (c) and (d), and 2D orthoslices (e), (f), (g) and (h) detailing the strut voids. Scaffolds were produced 0% porogen on the 90 ppi (a) and (e) and 45 ppi (b) and (f) and with the slurry containing 20% porogen on the 90 ppi (c) and (g) and 45 ppi (d) and (h) templates.

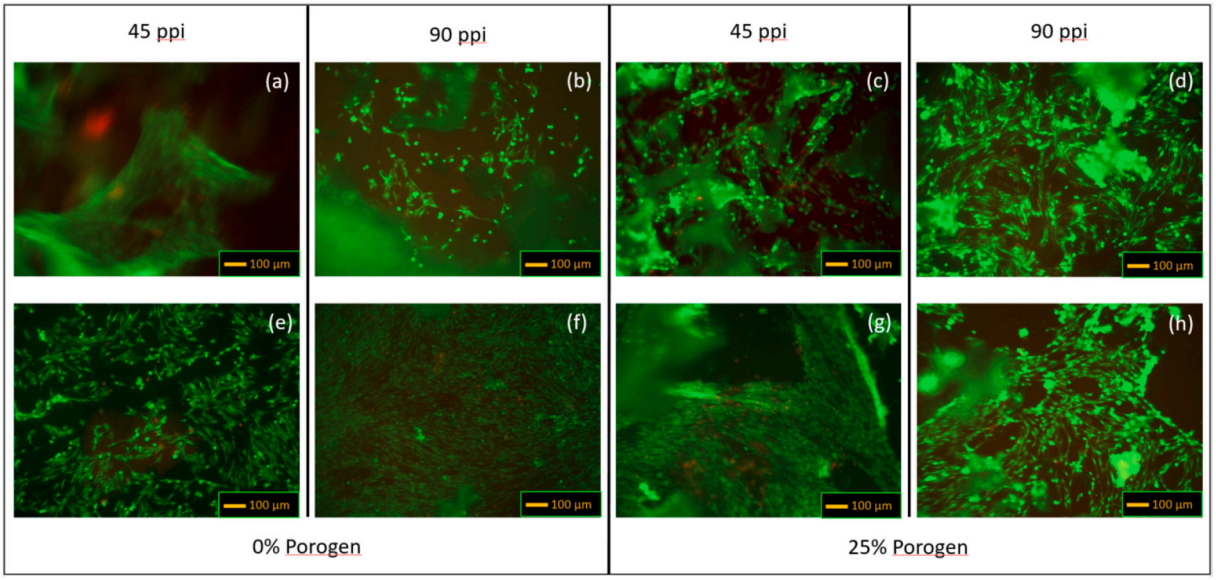

Fig. 3. Confocal microscopy images of scaffolds seeded with cells and stained with CalceinAM (green, live cells) and PI (red, dead cells) when produced using 0% porogen and the 45 ppi (a) and (e) and 90 ppi (b) and (f) and when produced with 25% porogen and the 45 ppi (c) and (g) and 90 ppi (d) and (h) when seeded for 1 d (a), (b), (c), and (d) and 3 d (e), (f), (g) and (h).

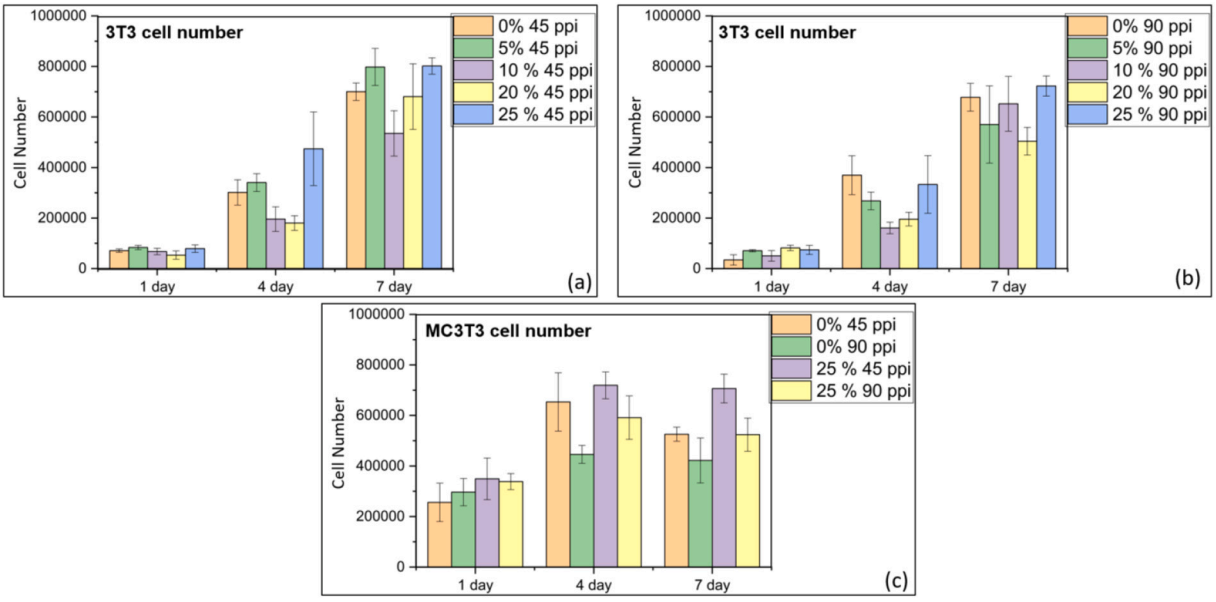

Fig. 4. Mean ± SD (n = 9) cell number as quantified by MTT assay for scaffolds produced using AFR from the 45 (a) and 90 ppi (b) templates when seeded with 3T3 cells and (c) MC3T3 cells.

significant improvement in attachment (Fig. 4c) compared to 3T3 cells. Again, use of the 45 ppi template led to a slightly higher number of cells compared to the 90 ppi template throughout the study. Incorporating porogen into the slurry led to a statistically significant ($P < 0.05$) increased number of cells in all cases except for the scaffold produced from the 45 ppi template at day 4. Finally, the maximum number of cells is similar to that seen on scaffolds seeded with 3T3 cells, indicating that the scaffolds are fully confluent and cannot support any more cells.

The ALP activity on scaffolds seeded with 3T3 and MC3T3 cells was quantified after 1, 4 and 7 days as shown in Fig. 5. When seeded with 3T3 cells, those produced with porogen had a significant improvement in the amount of ALP released after 4 days, whilst those fabricated without exhibited greater increases after 7 days. Furthermore, the template used to generate the scaffold did not greatly affect the amount of ALP released in any of the cases. It should be noted that there was a large range to the results for all conditions, causing there to be no statistical significance ($P > 0.01$) in almost all cases. These results suggest that the inclusion of the porogen had little effect on bone formation within this period.

Seeding scaffolds with MC3T3 cells had a similar effect on the level of ALP expressed; namely that the scaffolds produced with porogen exhibited a greater increase after 4 days, whilst those fabricated without porogen demonstrated a larger increase after 7 days. The template again had little effect on the amount of ALP released. It is also important to note that, as is to be expected, the levels of ALP expressed with the MC3T3 cells 1 day after seeding scaffolds produced without porogen was double that measured when 3T3 cells were seeded. This was accompanied by a reduction to the range of the results, although this was only

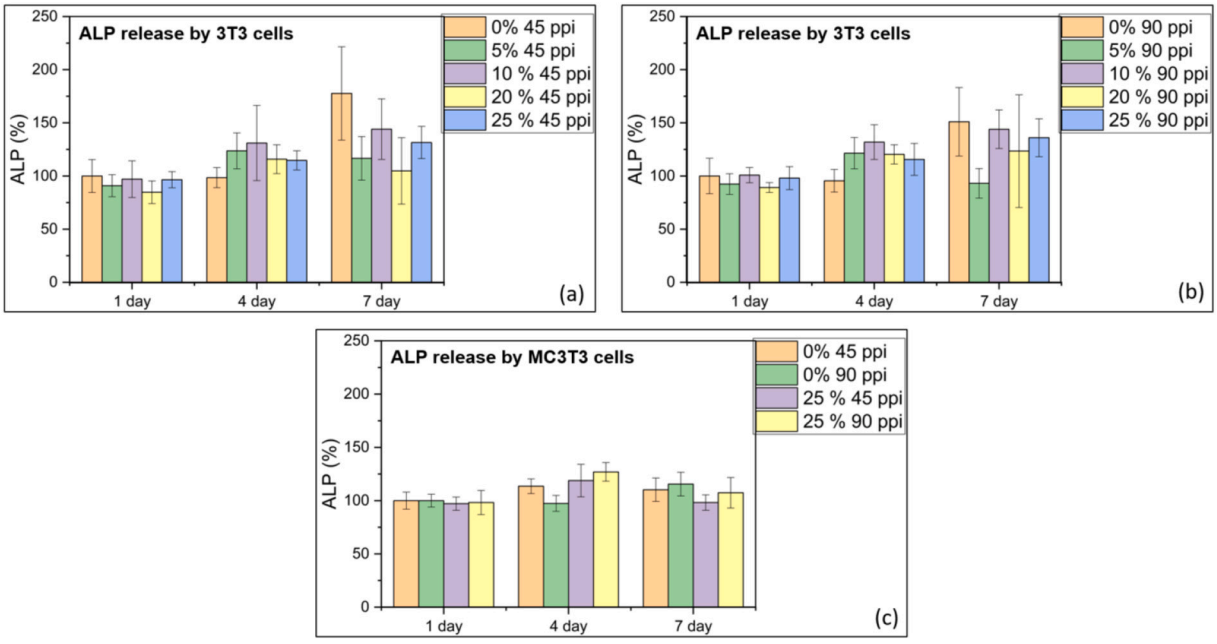

Fig. 5. Mean ± SD (n = 9) ALP released by scaffolds produced using the AFR from the 45 (a) and 90 ppi (b) templates with when seeded with 3T3 cells and (c) MC3T3 cells.

statistically significant after 7 days ($P < 0.05$).

The amount of calcium dissolution measured after 1, 4 and 7 days in PBS and DMEM increased with time for all scaffolds. This was minimally affected by the template used to fabricate the structure or the amount of porogen in the slurry, shown in Supplementary S2. There was a difference of 8 ± 1 mg/dl between equivalent scaffold submerged in PBS and DMEM, corresponding well with the 10 mg/dl calcium salts in DMEM after dilution and the measured calcium content of DMEM of 9 ± 0.2 mg/dl.

4. Discussion

4.1. Compressive strength

Measurements of bulk density can be used to infer the theoretical mechanical strength of a material [46], with the theoretical predictions of compressive yield stress calculated using Eq. (4) correlating well ($R^2 = 0.99$) with those obtained experimentally for scaffolds produced with and without porogen on the 45 ppi template and with no porogen on the 90 ppi template. There are no previous reports comparing the theoretical mechanical strength to experimental values for structures combining macro and microporosity, thus the strength of any sample which incorporates both types of porosity must be experimentally determined. The novel method of predicting the mechanical strength of scaffolds by considering the relationship between porosity and strength hypothesised in this work aimed to eliminate the requirement to destructively test each sample. However, the data obtained attempting to validate this theory suggests that incorporating a shape factor into a standard equation for determining the compressive strength of porous structures is not suitable for confidently predicting the yield strength of the sample as the there was a significant difference between the predicted (16.5 ± 1.7 kPa) and experimental (159 ± 61 kPa) values for the scaffold manufactured with 25% porogen in the slurry when using the 90 ppi template. However, as there is a relatively wide range in the yield strength values obtained experimentally, it is suggested that further investigation into this relationship would be advantageous. Particularly, the surface area could be a factor, as higher values could indicate less consolidation of the scaffold which would negatively impact the mechanical strength. This is supported by the surface area being much lower for the scaffold with 25% porogen in the slurry compared to the scaffolds produced with other porogen contents when using the 90 ppi template.

The mechanical strength of HA foams has been examined and investigated by others, with structures of equally high porosity having similar values of compressive strength, as shown in Table 4. However, in all cases this is much less than that of natural cancellous bone which ranges between 2 and 23 MPa [47]. Further investigations into the long-term *in-vivo* impact of implanting such scaffolds should be determined, as previous studies have not drawn any conclusive recommendations as to an optimised mechanical strength [48,49].

The increased yield stress when fabricating samples using a higher number of coats of the slurry on the template, or the 90 ppi template as opposed to the 45 ppi template correlates to the higher surface area. As shown in Table 3, the processing parameters had a greater effect on the theoretical mechanical strength when scaffolds were fabricated from the 90 ppi template compared to the 45 ppi template. The ratio of pore to strut size is less affected by coating the 45 ppi template multiple times as the change to the pore and strut size is relatively small for all structures. Therefore for structures with larger pores and struts, the ratio between the two is not as affected as for those with smaller pore and strut sizes. The shape factor is based on individual pore size alone. Micropore agglomeration when producing structures with higher camphene contents, as previously demonstrated [40], is therefore thought to contribute to the higher correlation between the experimental and theoretical values.

The values obtained for the theoretical compressive yield strength have been calculated using the bulk yield stress of HA. However, the

Table 4
Compressive yield stress of scaffolds fabricated using foam reticulation based techniques, with values obtained experimentally in this work compared to those available in the literature with similar porosities.

Porosity (%)	Yield stress (kPa)	Ref
85–94	5.7–159	Current study
95	7	[50]
83	110–230	[51]
80–90	<0.5	[52]
70	950	[9]

instability of HA during sintering above 900 °C can lead to the production of α–TCP, β-TCP or whitlockite [53] depending on material purity. Furthermore, previous work of the authors has shown that at least a partial phase change to whitlockite ($Ca_9Mg_{0.7}Fe^{2+}_{0.5}(PO_4)_6(PO_3OH)$) occurs [40], which has a 5% higher yield stress compared to HA [25]. This difference is within the error obtained for all scaffold strengths calculated theoretically, and hence the use of the value of yield stress for HA is considered appropriate herein.

4.2. Cell viability evaluation

Analysis was undertaken to determine whether incorporating a porogen had a positive effect on the biological performance of scaffolds, with scaffolds fabricated without any porogen used as the base against which their performance was analysed. It has been previously shown that these demonstrated increased cellular activity compared to a commercially available porous HA disc when seeded with osteoblast-like MG63 cells [38]. The elongated morphology of cells 24 h after seeding observed herein suggests that they had attached to the struts of the scaffolds, with viability similar to that observed prior to seeding. Thus, the structures offer a suitable surface onto which cells can grow, with viability similar to that observed with other conventional scaffold manufacturing techniques, as demonstrated by cytotoxicity assessment of gel-cast structures [54] and cell adhesion of Vero cells covering the surface of porous HA microcarriers fabricated by foam reticulation [55].

There was a significant reduction (70–80%) in the number of 3T3 cells 1 day after seeding, which is most likely to be due to cell detachment [56,57]. Some regions of the scaffolds exhibited little or no activity when observing the formazan production prior to its dissolution for analysis, as shown in Fig. 6. This may have been where the cells were aliquot, or potentially due to the lack of movement of media inhibiting the migration of cells throughout the structures. The increase in the number of MC3T3 cells 1 day after seeding lends more support to the hypothesis that the lack of movement of media is the cause for a decrease in cell number.

Both templates produced scaffolds with pore sizes within the range outlined for bone cell growth of 100–900 μm [2]. In most cases the template used did not significantly affect the cell count. However when seeded with the pre-osteoblast MC3T3 cells, the scaffolds from the 45 ppi template exhibited a higher number of cells compared to those from the 90 ppi template ($P < 0.01$), suggesting that the larger pore size may be more suited to bone regenerative applications. This should however be considered alongside the significantly reduced strength of these scaffolds, as additional protection may be required to ensure the scaffold maintains the structure for a suitable period.

The scaffolds produced with 25 wt% camphene inclusion exhibited a statistically significant increase in the number of 3T3 cells counted 7 days after seeding compared to those produced without camphene. No other level of camphene inclusion led to such improvements. The size of individual micropores is 2–3 μm, which is large enough to affect cell signalling and subsequent differentiation [56], but does not allow for capillary growth. Furthermore, the coalescence of micropores generating larger micropores of 20–30 μm may allow cell infiltration whilst individual micropores are smaller than cells and thus do not. It should be noted that this is influenced by the amount of porogen in the slurry, as higher camphene percentages increased micropore size, however the exact location is not controllable. Freeze drying the samples enables the microstructure to be controlled [7], whilst alternative porogens could also be used to vary the micropore size [6].

Whilst 3T3 cells are fibroblastic cells with little scope for changing their phenotype [58], the viability assays used herein demonstrate the intrinsic lack of cytotoxicity of the scaffolds. Whilst bone cells express ALP at greater concentrations than other cell types, it is expressed throughout the body. Indeed, ALP expression has been used as the basis of a cell quantification technique for, amongst others, 3T3 cells [59]. Thus, the assay used here may have been sensitive enough to show the base levels of ALP, with the increase in levels solely due to the increased cell number.

There are a number of osteogenic regulator genes, including ALP, runt-related transcription factor 2 (RUNX2), osterix (Osx), osteocalcin (OCN) and Collagen type 1 (Col-1) [60]. A renowned indicator of osteogenic differentiation [61,62], ALP is regularly used to identify the initial stages of osteogenesis [63], with changes to activity observed from as few as 5 days [64]. ALP is regulated by a complex, interconnected network of signalling pathways, including the BMP/RUNX2/Osx network and WNT signalling cascade, the exact mechanisms of which are not fully understood [63]. For example, upregulation of ALP has been found to correlate with Col-1 synthesis [65], which in turn has previously aligned with RUNX2 expression [66]. Another early indicator of osteogenesis, RUNX2 regulates the expression of downstream markers, such as OCN [67]. Herein, ALP has been measured, however as understanding of the role of different genes is increased, evaluation of the impact controlled hierarchical structures has on their expression may be required.

Meanwhile, MC3T3 cells can differentiate down osteoblastic lineages depending on the culture environment [68] and as such their viability is perhaps more important than that of 3T3 cells for bone reparative applications. Seeding scaffolds with MC3T3 cells led to similar observations as when 3T3 cells were seeded, demonstrating their osteogenicity and indicating that incorporating 25 wt% porogen enhances viability for bone regenerative applications.

Whilst only the level of calcium dissolution was measured, the amount of Ca^{2+} is linked with the amount of PO_4^{3-}. Beck et al. have shown how this regulates the release of osteopontin [68] and can alter

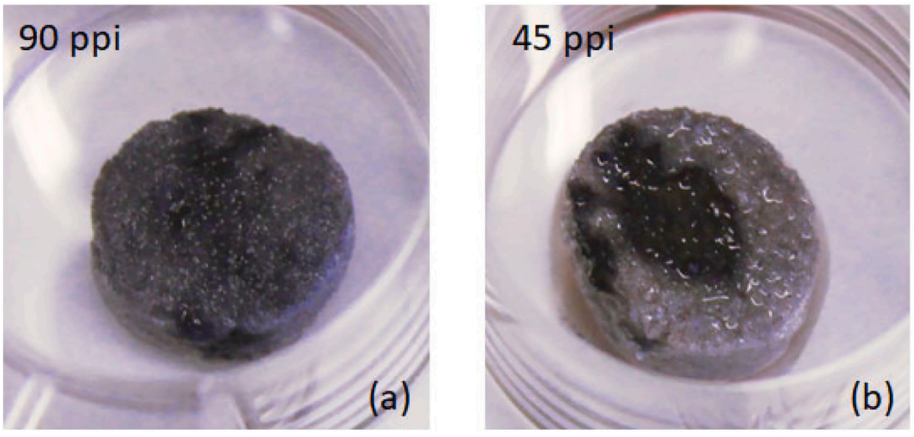

Fig. 6. Scaffolds (*ca.* 1 cm diameter) following formazan production on scaffolds fabricated from the (a) 90 ppi and (b) 45 ppi template, yet prior to dissolution.

gene expression [22], which may have caused subtle changes in 3T3 morphology causing ALP expression. Furthermore, this provides two possible explanations for the decrease in cells between days 4 and 7. The scaffolds could have become fully confluent and as such could not accommodate any more cell growth, although this is not supported by the presence of regions with little or no formazan production, Fig. 6. Alternatively, certain cells may have become more osteoblastic in nature, leading to the death of those without this potential. This explanation is supported by the evidence of the increase in the amount of ALP released per cell.

One final point of note is that Chang et al. [3] have already shown that foam reticulated structures exhibit enhanced bony growth compared to autografts *in-vivo*. This work has demonstrated that the presence of controllably produced microporosity enhances cell viability compared to non-microporous foam reticulated HA structures. Therefore, although this requires verification *via in-vivo* analysis, it suggests that structures fabricated *via* the AFR technique may offer a suitable alternative to grafting procedures.

5. Conclusions

Synthetic scaffolds offer an alternative to autografts as bone reparative aids, with the incorporation of a hierarchical structure combining micro and macroporosity potentially improving the cell viability and expression of osteogenic markers. Whilst the AFR, which combines freeze casting and foam reticulation, can produce scaffolds with a controllable macrostructure of microporous struts, the biological and mechanical properties comparing structures produced with and without micropores has not been previously investigated.

The porosity of samples was between 85 and 94% depending on template and porogen content. This has been used to calculate the theoretical compressive yield stress using the novel incorporation of a shape factor to allow for microporosity, of 3.7–134 kPa. However, the theoretical and experimental values exhibited significant differences, of up to 20% and hence it is suggested that further investigations into alternative methods of theoretically determining the yield stress are necessary, such as, for example, considering the surface area of the scaffolds. Whilst the strength of samples is weak compared to that of natural bone, it correlates well with other scaffolds of similarly high porosity.

Structures fabricated with no microporosity have previously been shown to exhibit an enhanced biological viability compared to a commercially available porous HA disc. Herein, the effect of incorporating camphene as a micropore generating porogen was investigated.

There was no statistically significant difference in the expression of the osteogenic marker ALP whether camphene was included as a porogen or not. Of greater interest was the expression of ALP with the use of fibroblastic 3T3 cells, albeit with some potential for differentiation down alternative lineages. Further investigations as to whether this is due to the assay or the initiation of osteoblastic differentiation are required. The scaffolds generated using the maximum level of porogen inclusion using the 45 ppi template demonstrated the greatest cell number after 7 days *in-vitro* culture. In addition, this was significantly greater ($P < 0.0005$) than from scaffolds fabricated without the inclusion of a porogen, indicating this has a positive effect on the biological activity initiated by the samples. Further *in-vivo* analyses are required however to definitively state whether the samples offer a suitable alternative to existing grafting procedures.

CRediT authorship contribution statement

James Winnett: Conceptualization, Methodology, Formal Analysis, Investigation, Writing – Original Draft, Funding Acquisition; **Neeraj Jumbu**: Methodology, Validation; **Sophie Cox**: Writing – Review & Editing; **Greg Gibbons**: Resources, Supervision, Project administration; **Liam Grover**: Resources, Supervision; **Jay Warnett**: Investigation, Formal Analysis, Visualization; **Mark A Williams**: Resources, Supervision; **Claire E J Dancer**, Resources, Writing – Review & Editing, Supervision, Project Administration; **Kajal K Mallick**: Conceptualization, Funding Acquisition.

The authors confirm that the material presented in this manuscript has not been previously published, including in abstract form, nor is it under consideration by any other journal.

Declaration of competing interest

The authors declare that they have no known competing financial interests or personal relationships that could have appeared to influence the work reported in this paper.

Acknowledgments

The authors are grateful to the Engineering and Physical Research Council (EPSRC) for supporting this work through Collaborative Research Student (CTA) [GR/T11371/0] and Standard Research Student (DTG) [EP/J500586/1] grants.

This paper is dedicated in memory of the life and work of Dr. Kajal K Mallick.

Appendix A. Supplementary data

Supplementary data to this article can be found online at https://doi.org/10.1016/j.bioadv.2022.212766.

References

[1] J. Planell, S. Best, D. Lacroix, A. Merolli, in: Bone Repair Biomaterials, Woodhead Publishing, UK, 2009, p. 464.
[2] K.J.L. Burg, S. Porter, J.F. Kellam, Biomaterial developments for bone tissue engineering, Biomaterials 21 (2000) 2347–2359.
[3] B.-S. Chang, C.-K. Lee, K.-S. Hong, H.-J. Youn, H.-S. Ryu, S.-S. Chung, et al., Osteoconduction at porous hydroxyapatite with various pore configurations, Biomaterials 21 (2000) 1291–1298.
[4] B. Annaz, K.A. Hing, M. Kayser, T. Buckland, L. Di Silvio, Porosity variation in hydroxyapatite and osteoblast morphology: a scanning electron microscopy study, J. Microsc. 215 (2004) 100–110.
[5] X. Lu, Y. Leng, Quantitative analysis of osteoblast behavior on microgrooved hydroxyapatite and titanium substrata, J. Biomed. Mater. Res. A 66 (2003) 677–687.
[6] B. Chuenjitkuntaworn, W. Inrung, D. Damrongsri, K. Mekaapiruk, P. Supaphol, P. Pavasant, Polycaprolactone/hydroxyapatite composite scaffolds: preparation, characterization, and in vitro and in vivo biological responses of human primary bone cells, J. Biomed. Mater. Res. A 94A (2010) 241–251.
[7] Q. Fu, M.N. Rahaman, F. Dogan, B.S. Bal, Freeze casting of porous hydroxyapatite scaffolds. I. Processing and general microstructure, J Biomed Mater Res B Appl Biomater 86 (2008) 125–135.
[8] S. Deville, Freeze-casting of porous ceramics: a review of current achievements and issues, Adv. Eng. Mater. 10 (2008) 155–169.
[9] E. Cunningham, N. Dunne, S. Clarke, S.Y. Choi, G. Walker, R. Wilcox, et al., Comparative characterisation of 3-D hydroxyapatite scaffolds developed via replication of synthetic polymer foams and natural marine sponges, Tissue Sci Eng S1 (001) (2011) 1–9.
[10] J. Yang, J. Yu, Y. Huang, Recent developments in gelcasting of ceramics, J. Eur. Ceram. Soc. 31 (2011) 2569–2591.
[11] D. Avnir, T. Coradin, O. Lev, J. Livage, Recent bio-applications of sol-gel materials, J. Mater. Chem. 16 (2006) 1013–1030.
[12] S.C. Cox, J.A. Thornby, G.J. Gibbons, M.A. Williams, K.K. Mallick, 3D printing of porous hydroxyapatite scaffolds intended for use in bone tissue engineering applications, Mater. Sci. Eng. C 47 (2015) 237–247.
[13] A. Butscher, M. Bohner, S. Hofmann, L. Gauckler, R. Muller, Structural and material approaches to bone tissue engineering in powder-based three-dimensional printing, Acta Biomater. 7 (2011) 907–920.
[14] J.M. Williams, A. Adewunmi, R.M. Schek, C.L. Flanagan, P.H. Krebsbach, S. E. Feinberg, et al., Bone tissue engineering using polycaprolactone scaffolds fabricated via selective laser sintering, Biomaterials 26 (2005) 4817–4827.
[15] F.E. Wiria, K.F. Leong, C.K. Chua, Y. Liu, Poly-epsilon-caprolactone/hydroxyapatite for tissue engineering scaffold fabrication via selective laser sintering, Acta Biomater. 3 (2007) 1–12.
[16] K.F. Leong, C.M. Cheah, C.K. Chua, Solid freeform fabrication of three-dimensional scaffolds for engineering replacement tissues and organs, Biomaterials 24 (2003) 2363–2378.

[17] F.J. Martinez-Vazquez, F.H. Perera, P. Miranda, A. Pajares, F. Guiberteau, Improving the compressive strength of bioceramic robocast scaffolds by polymer infiltration, Acta Biomater. 6 (2010) 4361–4368.
[18] J.R. Woodard, A.J. Hilldore, S.K. Lan, C.J. Park, A.W. Morgan, J.A. Eurell, et al., The mechanical properties and osteoconductivity of hydroxyapatite bone scaffolds with multi-scale porosity, Biomaterials 28 (2007) 45–54.
[19] S.J. Polak, S.K. Levengood, M.B. Wheeler, A.J. Maki, S.G. Clark, A.J. Johnson, Analysis of the roles of microporosity and BMP-2 on multiple measures of bone regeneration and healing in calcium phosphate scaffolds, Acta Biomater. 7 (2011) 1760–1771.
[20] J.Y. Rho, L. Kuhn-Spearing, P. Zioupos, Mechanical properties and the hierarchical structure of bone, Med. Eng. Phys. 20 (2) (1998) 92–102.
[21] D.T. Reilly, A.H. Burstein, Elastic and ultimate properties of compact bone tissue, J. Biomech. 8 (6) (1975) 393–397.
[22] J. Zhao, S.G. Xiao, X. Lu, J.X. Wang, J. Weng, A study on improving mechanical properties of porous HA tissue engineering scaffolds by hot isostatic pressing, Biomed. Mater. 1 (2006) 188–192.
[23] N. Koc, M. Timucin, F. Korkusuz, Fabrication and characterization of porous tricalcium phosphate ceramics, Ceram. Int. 30 (2) (2004) 205–211.
[24] K.K. Mallick, Freeze casting of porous bioactive glass and bioceramics, J. Am. Ceram. Soc. 92 (1) (2009) S85–S94.
[25] Q. Fu, M.N. Rahaman, B.S. Bal, R.F. Brown, Proliferation and function of MC3T3-E1 cells on freeze-cast hydroxyapatite scaffolds with oriented pore architectures, J. Mater. Sci. Mater. Med. 20 (5) (2009) 1159–1165.
[26] J. Kim, D. Lim, Y.H. Kim, Y.H. Koh, M.H. Lee, I. Han, S.J. Lee, O.S. Yoo, H.S. Kim, J. C. Park, A comparative study of the physical and mechanical properties of porous hydroxyapatite scaffolds fabricated by solid freeform fabrication and polymer replication method, Int. J. Precis. Eng. Manuf. 12 (4) (2011) 695–701.
[27] B. Chen, T. Zhang, J. Zhang, Q. Lin, D. Jiang, Microstructure and mechanical properties of hydroxyapatite obtained by gel-casting process, Ceram. Int. 34 (2) (2008) 359–364.
[28] Y. Gao, W.L. Cao, X.Y. Wang, Y.D. Gong, J.M. Tian, N.M. Zhao, X.F. Zhang, Characterization and osteoblast-like cell compatibility of porous scaffolds: bovine hydroxyapatite and novel hydroxyapatite artificial bone, J. Mater. Sci. Mater. Med. 17 (9) (2006) 815–823.
[29] A. Balamurugan, G. Balossier, S. Kannan, J. Michel, A.H.S. Rebelo, J.M.F. Ferreira, Development and in vitro characterization of sol-gel derived CaO-P2O5-SiO2-ZnO bioglass, Acta Biomater. 3 (2) (2007) 255–262.
[30] C.T. Wu, Y.X. Luo, G. Cuniberti, Y. Xiao, M. Gelinsky, Three dimensional printing of hierarchical and tough mesoporous bioactive glass scaffolds with a controllable pore architecture, excellent mechanical strength and mineralization ability, Acta Biomater. 7 (6) (2011) 2644–2650.
[31] Y. Shanjani, Y.X. Hu, R.M. Pilliar, E. Toyserkani, Mechanical characteristics of solid-freeform-fabricated porous calcium polyphosphate structures with oriented stacked layers, Acta Biomater. 7 (4) (2011) 1788–1796.
[32] F.P.W. Melchels, J. Feijen, D.W. Grijpma, A poly(D, L-lactide) resin for the preparation of tissue engineering scaffolds by stereolithography, Biomaterials 30 (23–24) (2009) 3801–3809.
[33] P. Miranda, A. Pajares, E. Saiz, A.P. Tomsia, F. Guiberteau, Mechanical properties of calcium phosphate scaffolds fabricated by robocasting, J. Biomed. Mater. Res. A 85A (1) (2008) 218–227.
[34] J. Russias, E. Saiz, S. Deville, K. Gryn, G. Liu, R.K. Nalla, A.P. Tomsia, Fabrication and in vitro characterization of three-dimensional organic/inorganic scaffolds by robocasting, J. Biomed. Mater. Res. A 83A (2) (2007) 434–445.
[35] J.A. Lewis, Direct ink writing of 3D functional materials, Adv. Funct. Mater. 16 (17) (2006) 2193–2204.
[36] J.A. Lewis, J.E. Smay, J. Stuecker, J. Cesarano, Direct ink writing of three-dimensional ceramic structures, J. Am. Ceram. Soc. 89 (12) (2006) 3599–3609.
[37] J. Winnett, K.K. Mallick, Porous 3D bioscaffolds by adaptive foam reticulation, Bioinspired Biomim. Nanobiomaterials 4 (1) (2015) 4–14.
[38] K.K. Mallick, J. Winnett, W. van Grunsven, J. Lapworth, G.C. Reilly, Three-dimensional porous bioscaffolds for bone tissue regeneration: fabrication via adaptive foam reticulation and freeze casting techniques, characterization, and cell study, J. Biomed. Mater. Res. A 100 (2012) 2948–2959.
[39] K.K. Mallick, J. Winnett, Preparation and characterization of porous Bioglass® and PLLA scaffolds for tissue engineering applications, J. Am. Ceram. Soc. 95 (2012) 2680–2686.
[40] J. Winnett, K. Mallick, Parametric characterization of porous 3D bioscaffolds fabricated by an adaptive foam reticulation technique, JOM 66 (2014) 590–597.
[41] K. Girstmair, G. Kirchner, Towards a completion of Archimedes' treatise on floating bodies, Expo. Math. 26 (2008) 219–236.
[42] J.Y. Wong, J.D. Bronzino, Biomaterials, CRC Press, Boca Raton, 2007.
[43] J.B. Patterson, E.C. Morris, Measurement of absolute water density, 1 oC to 40 oC, Metrologia 31 (1994) 227–288.
[44] L.J. Gibson, M.F. Ashby, B.A. Harley, Cellular Materials in Nature and Medicine, Cambridge University Press, Cambridge ; New York, 2010.
[45] L.F. Nielsen, Strength and stiffness of porous materials, J. Am. Ceram. Soc. 73 (1990) 2684–2689.
[46] L.J. Gibson, M.F. Ashby, in: Cellular Solids: Structure and Properties, Cambridge University Press, UK, 1997, p. 510.
[47] S. Prasadh, R.C.W. Wong, Unraveling the mechanical strength of biomaterials used as a bone scaffold in oral and maxillofacial defects, Oral Sci. Int. 15 (2) (2018) 48–55.
[48] P. Chocholata, V. Kulda, V. Babuska, Fabrication of scaffolds for bone-tissue regeneration, Materials 12 (4) (2019) 568.
[49] G. Muralithran, S. Ramesh, The effects of sintering temperature on the properties of hydroxyapatite, Ceram. Int. 26 (2000) 221–230.
[50] G.R. Beck Jr., B. Zerler, E. Moran, Phosphate is a specific signal for induction of osteopontin gene expression, Proc. Natl Acad. Sci. USA 97 (2000) 8352–8357.
[51] S. Teixeira, M.A. Rodriguez, P. Pena, A.H. De Aza, S. De Aza, M.P. Ferraz, et al., Physical characterization of hydroxyapatite porous scaffolds for tissue engineering, Mater. Sci. Eng. C 29 (2009) 1510–1514.
[52] I.-M. Hubg, W.-J. Shih, M.-H. Hon, M.-C. Wang, The properties of sintered calcium phosphate with [CA]/[P] = 1.50, Int. J. Mol. Sci. 13 (10) (2012) 13569–13586.
[53] P. Sepulveda, J.G.P. Binner, S.O. Rogero, O.Z. Higa, J.C. Bressiani, Production of porous hydroxyapatite by the gel-casting of foams and cytotoxic evaluation, J. Biomed. Mater. Res. 50 (2000) 27–34.
[54] I. Sopyan, M. Mel, S. Ramesh, K.A. Khalid, Porous hydroxyapatite for artificial bone applications, Sci. Technol. Adv. Mater. 8 (2006) 116–123.
[55] D. Perizzolo, W.R. Lacefield, D.M. Brunette, Interaction between topography and coating in the formation of bone nodules in culture for hydroxyapatite- and titanium-coated micromachined surfaces, J. Biomed. Mater. Res. 56 (2001) 494–503.
[56] J.E. Davies, Bone bonding at natural and biomaterial surfaces, Biomaterials 28 (2007) 5058–5067.
[57] L.D. Charles, D.A. Yohay, L.W. Lever, R. Caton, R.J. Wenstrup, Distinct proliferative and differentiated stages of murine MC3T3-E1 cells in culture: an in vitro model of osteoblast development, J. Bone Miner. Res. 7 (1992) 683–692.
[58] A. Ben-Ze'ev, Animal cell shape changes and gene expression, BioEssays 13 (2005) 207–212.
[59] L.I. Huschtscha, F.C. Lucibello, W.F. Bodmer, A rapid micro method for counting cells "in situ" using a fluorogenic alkaline phosphatase enzyme assay, In Vitro Cell. Dev. Biol. 25 (1989) 105–108.
[60] W. Huang, S. Yang, J. Shao, Y.-P. Li, Signaling and transcriptional regulation in osteoblast commitment and differentiation, Front. Biosci. 12 (2007) 3068–3092.
[61] S. Trivedi, K. Srivastava, A. Gupta, T.S. Saluja, S. Kumar, D. Mehrota, S.K. Singh, A quantitative method to determine osteogenic differentiation aptness of scaffold, J. Oral. Biol. Craniofac. Res. 10 (2) (2020) 158–160.
[62] C. Yang, X. Gao, M.R. Younis, N.T. Blum, S. Lei, D. Zhang, Y. Lui, P. Huang, J. Lin, Non-invasive monitoring of in vivo regeneration based on alkaline phosphatase-responsive scaffolds, Chem. Eng. J. 408 (2021), https://doi.org/10.1016/j.cej.2020.127959.
[63] S. Vimalraj, Alkaline phosphatase: Structure, expression and its function in bone mineralisation, Gene 754 (2020), https://doi.org/10.1016/j.gene.2020.144855.
[64] J. Li, L. Hao, J. Wu, J. Zhang, J. Su, Linarin promotes osteogenic differentiation by activating the BMP-2/RUNX2 pathway via protein kinase-a signaling, Int. J. Mol. Med. 37 (4) (2016) 901–910.
[65] T. Ramesh, Osteogenic differentiation potential of human bone marrow-derived mesenchymal stem cells enhanced by bacoside-a, Cell Biochem. Funct. 39 (2021) 148–158.
[66] J. Wo, S.-S. Huang, D.-W. Wu, J. Zhu, Z.-Z. Li, F. Yuan, The integration of pore size and porosity distribution on ti-6Al-4V scaffolds by 3D printing in the modulation of osteo-differentiation, J. Appl. Biomater. Funct. Mater. 18 (2020) 1–10.
[67] W. Gong, Y. Dong, S. Wang, X. Gao, X. Chen, A novel nano-sized bioactive glass stimulates osteogenesis via the MAPK pathway, RSC Adv. 7 (2017) 13760–13767.
[68] G.R. Beck Jr., E. Moran, N. Knecht, Inorganic phosphate regulates multiple genes during osteoblast differentiation, including Nrf2, Exp. Cell Res. 288 (2003) 288–300.